NeuroImage 62 (2012) 1939–1946

Contents lists available at SciVerse ScienceDirect

NeuroImage

journal homepage: www.elsevier.com/locate/ynimg

Whole brain, high resolution spin-echo resting state fMRI using PINS multiplexing at 7 T

Peter J. Koopmans [a,b,*,1], Rasim Boyacioğlu [b,1], Markus Barth [a,b], David G. Norris [a,b,c]

[a] Erwin L. Hahn Institute for Magnetic Resonance Imaging, UNESCO-Weltkulturerbe Zollverein, Leitstand Kokerei Zollverein, Arendahls Wiese 199, D-45141 Essen, Germany
[b] Radboud University Nijmegen, Donders Institute for Brain, Cognition and Behaviour, Donders Centre for Cognitive Neuroimaging, Trigon 204 P.O. Box 9101, NL-6500 HB Nijmegen, The Netherlands
[c] MIRA Institute for Biomedical Technology and Technical Medicine, University of Twente, NL-7500 AE Enschede, The Netherlands

ARTICLE INFO

Article history:
Accepted 30 May 2012
Available online 6 June 2012

Keywords:
fMRI
Resting state
Spin echo
7 Telsa
Multiplexing
PINS

ABSTRACT

This article demonstrates the application of spin-echo EPI for resting state fMRI at 7 T. A short repetition time of 1860 ms was made possible by the use of slice multiplexing which permitted whole brain coverage at high spatial resolution (84 slices of 1.6 mm thickness). Radiofrequency power deposition was kept within regulatory limits by use of the power independent of number of slices (PINS) technique. A high in-plane spatial resolution of 1.5 mm was obtained, while image distortion was ameliorated by the use of in-plane parallel imaging techniques. Data from six subjects were obtained with a measurement time of just over 15 min per subject. A group level independent component (IC) analysis revealed 24 non-artefactual resting state networks, including those commonly found in standard acquisitions, as well as plausible networks for a broad range of regions. Signal was measured from regions commonly rendered inaccessible due to signal voids in gradient echo acquisitions. Dual regression was used to obtain spatial IC maps at the single subject level revealing exquisite localisation to grey matter that is consistent with a high degree of T_2-weighting in the acquisition sequence. This technique hence holds great promise for both resting state and activation studies at 7 T.

Introduction

Early in the history of BOLD fMRI, it was shown that T_2-weighted imaging should emphasise functional signal changes in the microvasculature, based on the finding that the contribution of extravascular dephasing around larger post capillary vessels is largely eliminated in T_2-weighted compared to T_2^*-weighted fMRI (Boxerman et al., 1995; Ogawa et al., 1993). Consequently, the use of T_2-weighted fMRI is desirable for the sake of a higher spatial specificity of BOLD activation. Owing to its high sensitivity, ready availability and (in relation to pure spin echo sequences) low radiofrequency power deposition SE-EPI is the most promising candidate sequence, but several alternatives have also been tested [FSE (Constable et al., 1994), RASER (Chamberlain et al., 2007), nb-S2-SSFP (Barth et al., 2010), HASTE (Poser and Norris, 2007), STE (Goerke et al., 2007), bSSFP (Miller et al., 2003; Scheffler et al., 2001)]. Unfortunately, the application of a sufficiently fast, whole brain SE-EPI protocol faces several practical limitations that have impeded the common use of T_2-weighting for fMRI:

i. In order to obtain the best possible sensitivity for SE-EPI one needs to measure the signal at an echo time corresponding to T_2 of grey matter which ranges from 60 to 80 ms depending on the specific magnetic field strength. This leads to a significantly longer TE than for GE imaging and consequently to a longer measurement time due to the lower efficiency of the sequence.
ii. The improvement in spatial specificity comes at the expense of functional sensitivity and is also due to reduced large vein effects. The drop in sensitivity of SE-EPI based fMRI has been shown to be significant (about a factor of 3 at 3 T) compared to its GE counterpart (Jochimsen et al., 2004; Norris et al., 2002). To compensate for (part of) the low sensitivity high field strengths have been advocated (Lee et al., 1999; Yacoub et al., 2003).
iii. The elimination of the static averaging contribution to the BOLD signal through the use of a spin-echo leaves contributions from both the well-localised extravascular dynamic averaging contribution originating from the capillary bed and smaller vessels, and from the intravascular compartment. At 3 T the gain in spatial specificity is hence limited (Parkes et al., 2005), and a further argument for the use of ultra high field strengths such as 7 T and

Abbreviations: IC, independent component; PINS, power independent of number of slices; RSN, resting state network.

* Corresponding author at: Radboud University Nijmegen, Donders Centre for Cognitive Neuroimaging, Trigon 240, Kapittelweg 29, NL-6525 EN Nijmegen, The Netherlands. Fax: +31 24 36 10652.
E-mail address: peter.koopmans@donders.ru.nl (P.J. Koopmans).

[1] Contributed equally to this work.

1053-8119/$ – see front matter © 2012 Elsevier Inc. All rights reserved.
doi:10.1016/j.neuroimage.2012.05.080

above is the virtual disappearance of the intravascular compartment owing to the short T_2 of venous blood at these field strengths (Lee et al., 1999; Yacoub et al., 2003).

iv. Last, but not least, the refocusing pulses may lead to very high SAR levels at field strengths of 7 T or above that either prohibit whole brain coverage or lead to restrictively long volume TRs. This SAR restriction unfortunately pertains at just the field strengths where the greatest benefit from spin-echo BOLD could be expected.

Due to these restrictions a whole brain protocol at 7 T with acceptable volume acquisition times and a sufficient spatial resolution to benefit from the higher SE specificity has hitherto proven impossible to realise. Recently, the development of multiplexed acquisition for EPI opened the possibility to speed up 2D multi-slice acquisitions considerably (Moeller et al., 2010) which has the potential to dramatically improve the efficiency of the sequence and hence reduce volume acquisition times. However, the SAR level of the multiplexed RF pulses increases linearly with the acceleration factor, which in combination with the requirement for short repetition times leads to prohibitively high SAR levels. In this study we implemented PINS RF pulses (Norris et al., 2011) for excitation and refocusing to overcome the above mentioned experimental limitations. We show that this enables the implementation of a whole brain SE-EPI protocol at 7 T with a spatial resolution of $1.5\times1.5\times1.6$ mm^3 within a volume acquisition time of less than 2 s while remaining within regulatory SAR levels. We use this technique to obtain resting state data from healthy subjects at 7 T.

Methods

Acquisition

Six right-handed subjects (5 male) were scanned after informed consent was given according to the guidelines of the local ethics committee. 2D SE-EPI scans were obtained using a 7 T MR scanner (Magnetom, Siemens Healthcare, Erlangen, Germany) equipped with a 32 channel head coil (Nova Medical, Wilmington, USA). Before acquiring multiplexed PINS resting state data, five volumes of non-multiplexed reference data were acquired, the average of which was used to calculate the reconstruction kernel (see: Reconstruction and registration). With the exception of the RF pulses used and the volume TR, the parameters of these two protocols were identical: TE 53 ms, sagittal orientation, phase encoding direction AP, matrix 160×160, voxel size 1.5×1.5 mm^2, 1.6 mm slice thickness with a 25% gap, flip angle 90°, PE-GRAPPA factor 3, bandwidth 1562 Hz/pixel, 40.3 ms readout train. Non-selective fat suppression was applied.

For the reference data conventional sinc RF pulses with the same bandwidth and duration as the PINS pulses mentioned below were used. The whole head was covered by 84 slices which led to a volume TR of 7430 ms. After the reference scan, the RF pulses were replaced by PINS pulses that allow multiple slices to simultaneously be excited/refocused with a considerable reduction in SAR compared to standard RF multiplexing techniques (Norris et al., 2011). PINS pulses consist of a series of RF hard pulses interleaved with slice selection gradient blips. The time integral of an individual blip is chosen such that it dephases the signal by 2π over the desired slice spacing thus creating a periodic slice profile. The amplitude of each of the hard pulses can be determined by a Fourier series expansion of the desired slice profile. Whereas periodicity may seem to imply an infinite number of slices, this is limited in practice by the extent of the subject's head or the transmit/receive volume(s) of the coil(s). Compared to the original single slice pulse there is an increase in SAR because part of the pulse duration is spent on gradients and not RF. This increase is however of a much lower magnitude than the increase in power deposition of a conventional multiplexed (summed) pulse which is proportional to the number of slices. Due to slew-rate limitations, PINS pulses have a relatively low bandwidth-time product (BWTP). To compensate for this we used RF pulse lengths of 7.68 ms for all RF pulses (excitation and refocusing, PINS and conventional pulse types) in order to achieve the desired slice thickness, allowing 35 sub-pulses to be used for a BWTP of 1.33. The multiplexed PINS acquisition used 21 stacks of slices with an inter-slice spacing of 42 mm. Consequently, the four-fold slice multiplexed acceleration reduced the volume TR to 1860 ms, allowing the acquisition of 500 volumes of high resolution SE resting state data in just over 15 min without exceeding SAR regulations.

Structural scans were acquired using MP2RAGE (Marques et al., 2010). Parameters were: matrix 320×320, 192 slices, voxel size $0.75\times0.75\times0.75$ mm^3, flip angles 4° and 5°, inversion times 900 and 3200, TE 2.04 ms, TR 5000, bandwidth 240 Hz/pixel, PE-GRAPPA factor 2. For two subjects (2 and 4) structural MP-RAGE data were already available from a different study (3 T Siemens Trio scanner, 32 channel head coil, matrix 256×256, 192 slices, TI 1100, TR 2300, flip angle 8°, bandwidth 130 Hz/pixel).

Reconstruction and registration

Both the 84 slice reference data and the 21 stack PINS data were first reconstructed in the phase encode direction using a 7×6 GRAPPA kernel (Griswold et al., 2002). Subsequently, the collapsed slices were disentangled using the SENSE-GRAPPA method (Blaimer et al., 2006) using a 5×4 kernel. Resting state data were realigned using SPM8 (http://www.fil.ion.ucl.ac.uk/spm/). We applied a distortion correction co-registration algorithm to map the EPI to the MP2RAGE data for each subject (Studholme et al., 2000; Visser et al., 2010). Based on normalised mutual information of the average EPI volume and the MP2RAGE this routine simultaneously estimated both the rigid body transformation parameters and the non-linear transformation in the phase-encode direction of the EPI data. In order to perform a group ICA this transformation was followed by registration to the MNI-152 T_1 template using FSL-FLIRT (Jenkinson et al., 2002). An example of a single volume before and after distortion correction is shown in Fig. 1.

Resting state analysis

Spatial smoothing was applied to the registered resting state data using a 5 mm kernel. Temporal drift was removed with a high-pass filter with a 100 s cut off. Group ICA was carried out with the multi-session temporal concatenation option of MELODIC v3.1 (Beckmann et al., 2005) with 70 components, a number similar to those used in previous resting state studies (Feinberg et al., 2010; Kiviniemi et al., 2009).

ICs from the group ICA which were identified as resting state networks (RSNs) are presented in figures in the Results section as overlays on the T1 weighted MNI-152 standard brain. The coordinates are in MNI space and images are shown in radiological convention. The most representative slices in three directions were chosen by either placing them on the z-score's centre-of-mass for ICs with a single or dominant cluster, or on the voxel with the peak z-score for ICs that consisted of distributed clusters where the centre-of-mass was in empty slices in between. The threshold for all ICs was set at 4.

Artefactual components were identified by examining each component's frequency spectrum (predominant RSN power should be concentrated below 0.1 Hz) and spatial location (ICs should be found in grey matter). RSN interpretation was achieved using previous group ICA studies with similar model orders (Kiviniemi et al., 2009; Varoquaux et al., 2010) and the Jülich histological (Eickhoff et al., 2007) and Harvard–Oxford cortical structural atlases (http://www.cma.mgh.harvard.edu/).

The components in Fig. 5 do not belong to the commonly reported RSNs, but also did not show any signs of artefacts. To interpret these the NeuroSynth database (Yarkoni et al., 2011) was consulted to

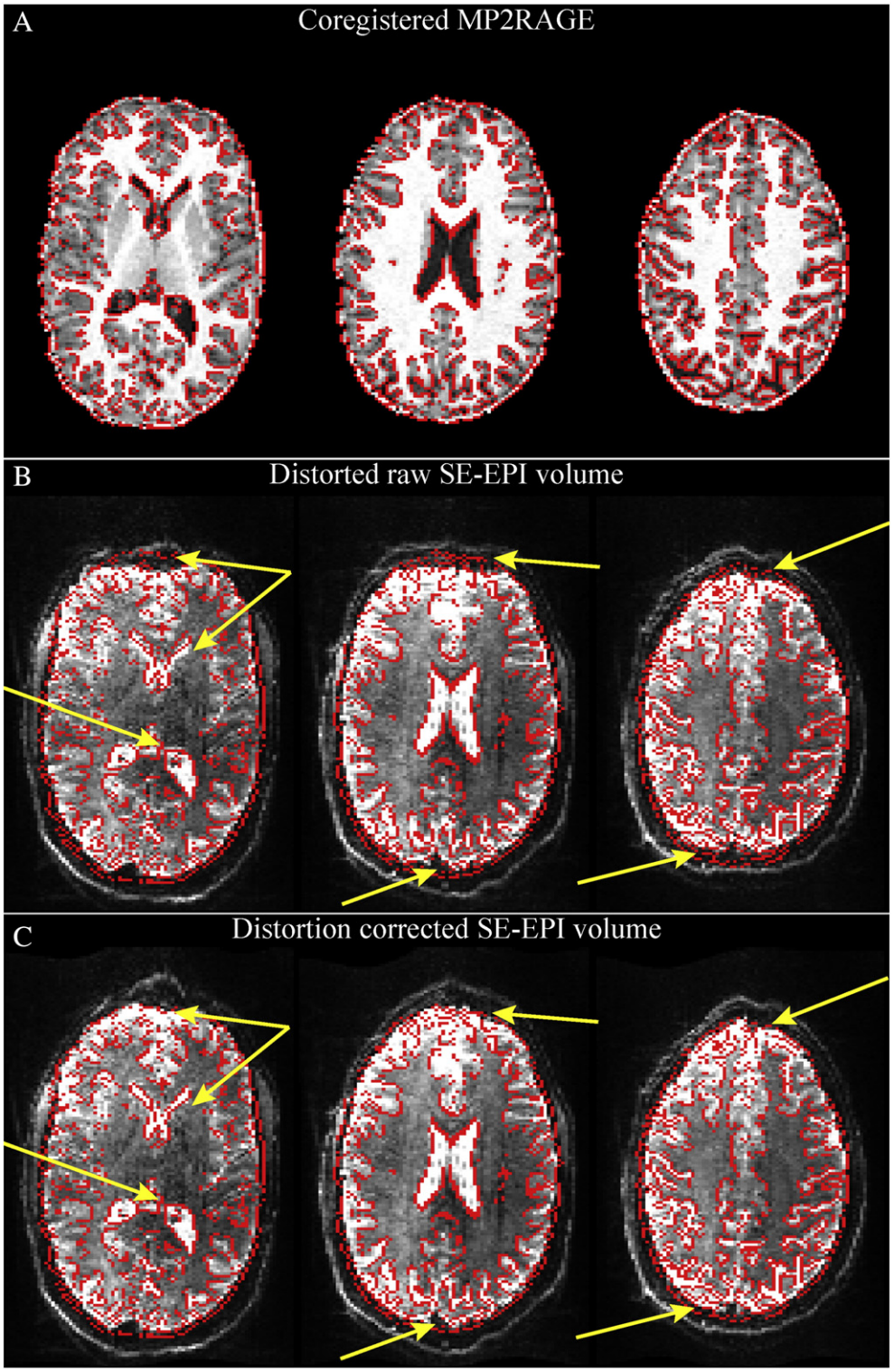

Fig. 1. Single subject example of the distortion correction. Three transversal slices are shown spaced 10 slices apart (15 mm) in the native resolution of the EPI data. A) The structural MP2RAGE scan and its edges as detected using the FSL-slicer tool. B) A single EPI volume before distortion correction. The edges detected in A are overlaid and clearly the overlap is suboptimal as indicated by the yellow arrows. C) The same volume after distortion correction. Most geometric distortion problems have been alleviated, the EPI data showing excellent overlap with the MP2RAGE.

compare the ICs spatial maps with known neuroimaging results and lists in which functions these ICs are implied. For each component in Fig. 5 a list of studies reporting activation foci within 10 mm of the IC's centre of mass was extracted and the most common functional associations are reported for each IC in the Results section.

To investigate the output of the group ICA at the individual subject level the dual regression approach is used (Beckmann et al., 2009). In this method, the resulting group level ICs are used as spatial regressors in a GLM to obtain subject-specific time courses of each component. These time courses are subsequently used as

temporal regressors in a second GLM to extract subject specific IC maps. In order to preserve the original resolution of the data as far as possible, this second GLM was applied to the resting state data in subject-space (i.e. without normalisation to MNI-152 and without 5 mm spatial smoothing).

Results

Fig. 2 illustrates ten typical, well known RSNs, demonstrated by many resting state studies (for an overview see: Smith et al., 2009). The default mode network (DMN), IC 52, contains mainly the posterior part of the regular DMN. The anterior part of the DMN is contained in components shown in Fig. 3. This separation of the DMN into separate posterior and anterior components is quite common for RSN studies with high model order (Kiviniemi et al., 2009). The visual areas are separated into three components, namely occipital pole, medial and lateral visual areas. The motor areas are split into four ICs. IC 5 is usually referred to as the midline feet area and covers postcentral gyrus, precentral gyrus and superior parietal lobe. Even though IC 5 is related to the primary somatosensory cortex in both hemispheres, it is connected to the primary cortex only in the right hemisphere. The other components with representations in the primary motor and somatosensory cortices are the ICs 24 and 31, which both include the hand area. They span the supramarginal gyrus, the postcentral gyrus and the anterior part of the superior parietal lobule. The last component from the motor area, IC 28, is composed of the primary and secondary somatosensory cortices, the primary motor cortex and the primary auditory cortex.

Fig. 3 shows seven ICs (1, 6, 7, 8, 22, 27 and 40) covering most of the frontal lobe. ICs 6 and 8 cover the medial prefrontal cortex (mPFC) and are situated at the anterior medial wall. They both extend into the superior frontal gyrus and the paracingulate gyrus. IC 1 can be labelled as superior PFC as it contains the frontal pole and the superior frontal gyrus. IC 7 is the anterior PFC including the superior frontal gyrus and extending into the middle frontal gyrus. IC 22 and IC 27 incorporate the orbito-frontal cortex. IC 40 contains the ACC and extends into the ventro-medial prefrontal cortex (vmPFC).

Fig. 4 shows three fairly large, left lateralised networks that include regions associated with language. IC 13 includes the pars opercularis, pars triangularis, precentral gyrus, postcentral gyrus, temporal pole and superior temporal gyrus. It is situated in Broca's area (Tomasi and Volkow, in press) centred on BA 44 and protrudes

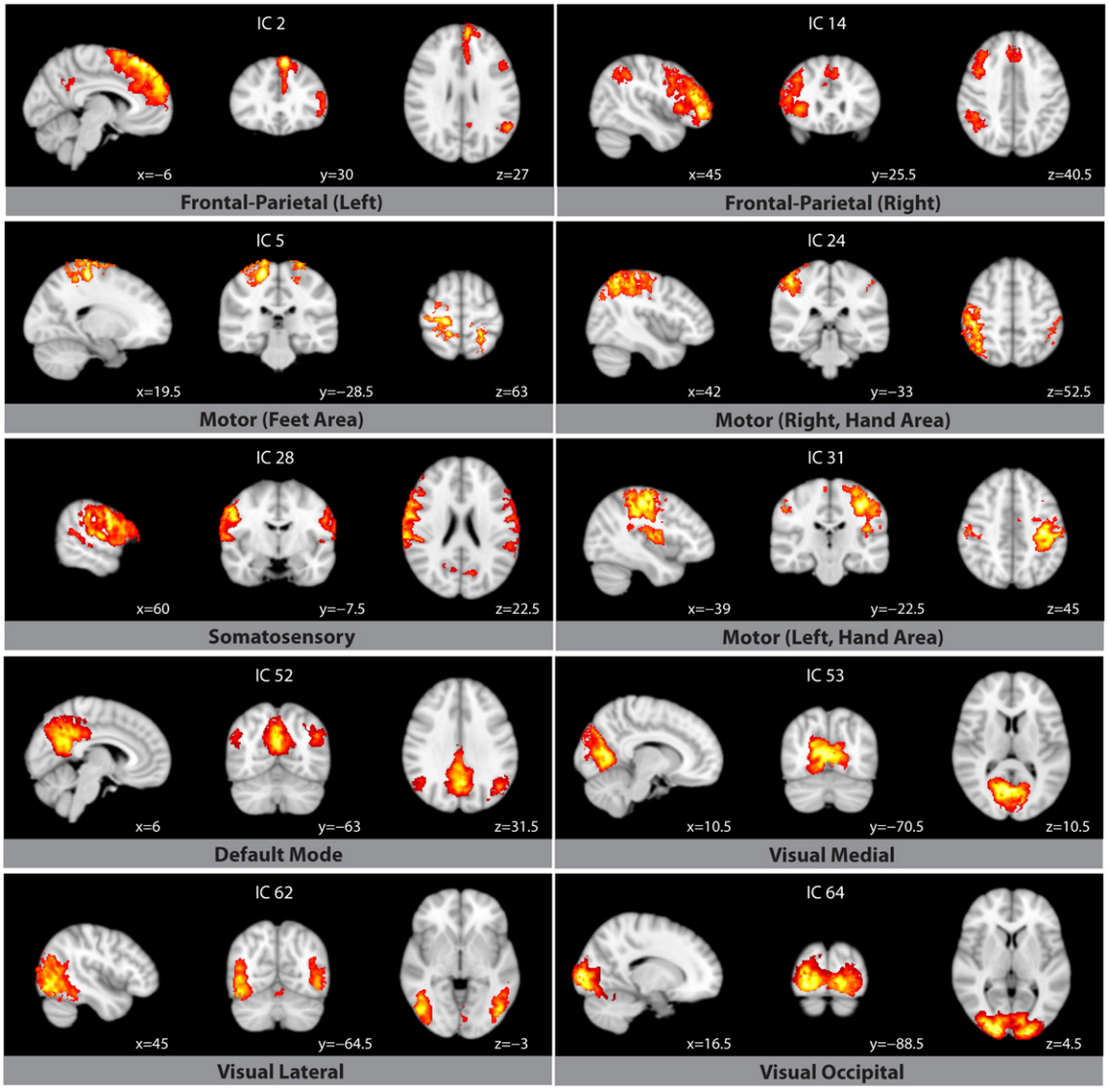

Fig. 2. Ten components of the ICA that are commonly found including left and right fronto-parietal, four motor, and three visual components as well as the DMN.

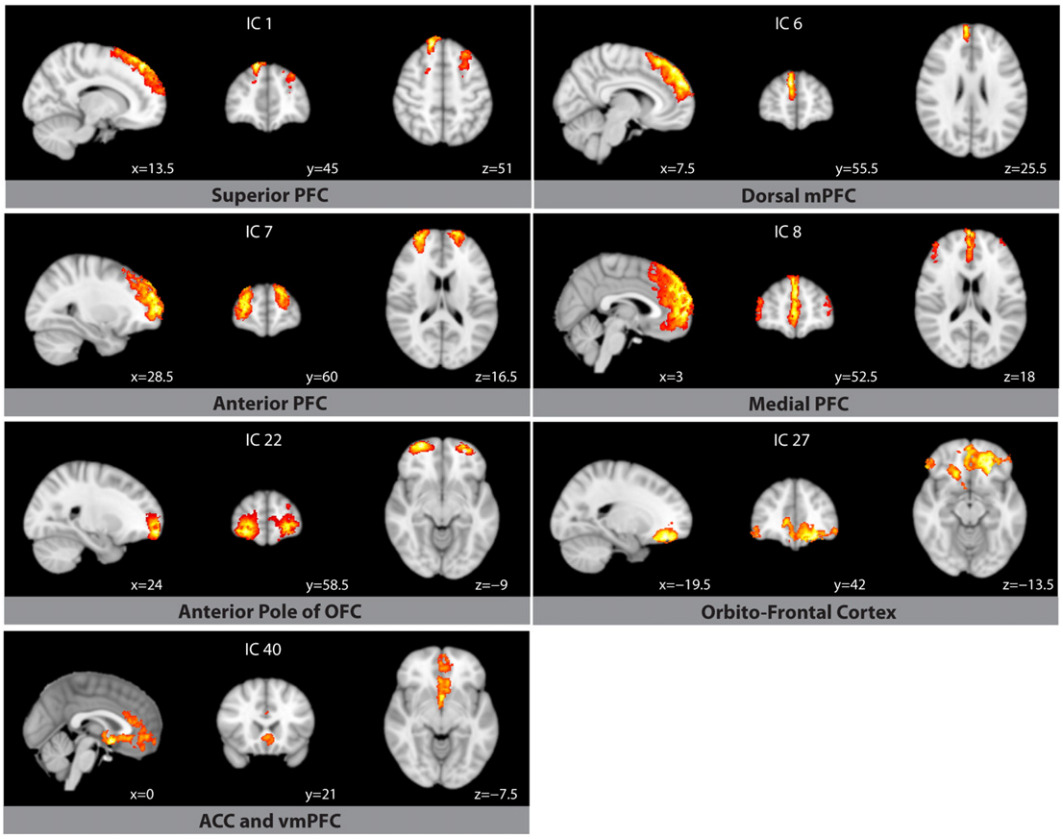

Fig. 3. ICs located in the frontal lobe. Owing to the reduced dropout of the spin echo method, ICs can be found in the inferior part of the frontal lobe, i.e. the orbito-frontal PFC.

into BA 45. IC 25, another component related to Broca's area, is more anterior with respect to IC 13 and is centred on BA 45. It incorporates the pars opercularis, the middle frontal gyrus and the frontal pole. IC 29 is composed of the middle temporal gyrus, the angular gyrus, the supramarginal gyrus and the parietal operculum cortex and includes Wernicke's area.

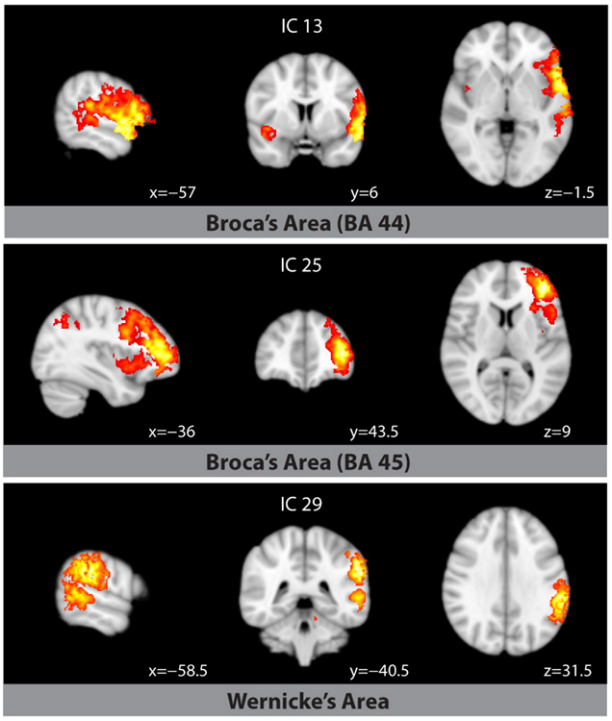

Fig. 4. ICs related to language processing. Please note the separation of Broca's area into BA 44 and 45, and the strong left-lateralisation of the language network (images shown according to radiological convention).

Additional, less commonly reported RSNs are illustrated in Fig. 5. These have been interpreted using the NeuroSynth database. IC 4 is situated at the superior and inferior division of the lateral occipital cortex and extends into the angular gyrus. The focus of IC4 corresponds to fMRI studies related to human face/voice recognition and processing, emotional/working memory encoding and vocal pitch processing. IC 37 is present at the inferior parietal lobule (supramarginal and angular gyrus) and the temporal lobe (superior and middle temporal gyrus). Its centre of mass is mainly located at the posterior superior temporal sulcus (pSTS) and this area is linked to functional studies related to human gaze, social interaction, joint/spatial attention, facial and emotional expression recognition and processing, and biological motion. IC 38 is Heschl's gyrus and its spatial map is associated with speech, speechreading, sentence comprehension and acoustic/sound processing. In both hemispheres IC 61 incorporates the lateral occipital cortex and extends to the superior parietal lobe, which spans to the premotor cortex (BA 6). The spatial map of IC 61 was virtually identical to ones of the superior parietal lobule (SPL) and intraparietal sulcus (IPS) in the NeuroSynth database. These two areas have been detected with functional paradigms such as word/numerical processing, mnemonic recoding, working memory, motor imagery, mental rotation, action/object perception and visuospatial processing.

To investigate the localisation of RSNs reported above, we used the dual regression approach to obtain unsmoothed high resolution maps on the single subject level. An example is shown in Fig. 6 for IC 28 which contains the somatosensory network for all subjects.

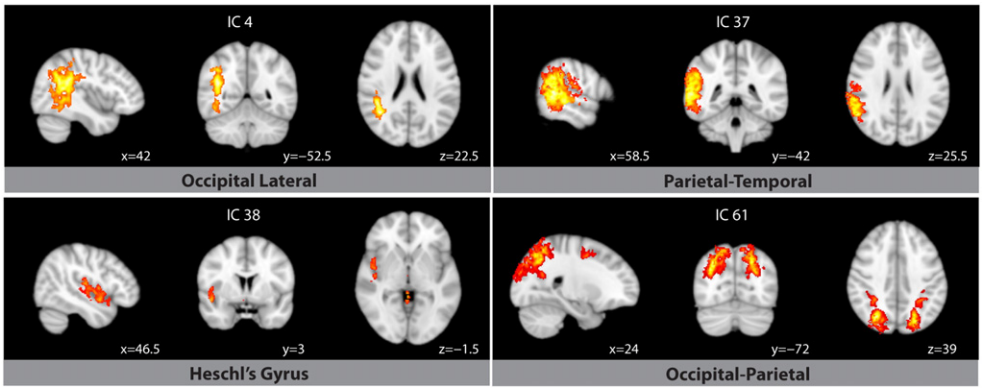

Fig. 5. Additional RSNs that do not belong to any of the categories shown in Figs. 2–4 but are not identified as artefacts. These RSNs were looked up in the neuroimaging meta-analysis database NeuroSynth and their implied functions are listed in the Results section.

Discussion

This article demonstrates the application of spin-echo EPI for resting state studies at 7 T. To fully benefit from the high specificity of SE, high resolution data were required to reduce partial volume effects. The use of PINS RF pulses combined with slice multiplexing makes it possible to obtain data at both a high temporal (TR<2 s) and spatial (<2 mm) resolution. The in-plane acceleration obtained using the GRAPPA technique permits a relatively short readout train (40.3 ms) and hence limits both the degree of T_2^* contamination and the image distortion. The resulting images are free of the signal voids that persistently confound gradient echo sequences hence making the whole brain accessible to this technique. The contrast in the images is a mixture of T_2 plus an undetermined contribution from T_2^*. The relatively small variation in the T_2-values of grey matter throughout the brain implies that acquisition at a single TE can be near optimal for all regions. Given the well known arguments pertaining to the near disappearance of the intravascular contribution to the spin-echo signal in veins at 7 T caused by the very short T_2 of venous blood (Lee et al., 1999; Yacoub et al., 2003) it is to be expected that the BOLD signal change in this experiment will arise mostly from the extravascular compartment. The simulations by Uludag et al. (2009) show that some intravascular effects may remain but that these are found in blood vessels with high (but not saturated) blood oxygenation levels (Y). However, this is only the case for capillaries (for which Y in rest is around 77%) and therefore these intravascular effects are not detrimental to the spatial specificity. There will be a major contribution from extravascular dynamic averaging about the capillaries and smaller vessels (the T_2-component) plus some static dephasing about the larger vessels (the unknown T_2^* contribution). Although the precise contrast is difficult to determine owing to the indeterminate degree of T_2^*-weighting, it can generally be claimed that the recorded signal changes will be closer to the site of neuronal activation than for a gradient echo sequence, because the relative contribution of the dynamic averaging will always be higher for spin-echo acquisition. If the contrast were that of a pure spin-echo then it could be argued that the greatest signal intensity would then arise from vascular layer III (Norris, 2012). It is hence consistent with this line of argument that the single subject, high resolution results shown in Fig. 6 demonstrate a convincing localisation of the ICs to the grey matter.

To date spin-echo EPI has not been utilised for resting state fMRI. The reasons for this are readily apparent: at lower field strengths there is little benefit to be obtained from using spin-echo (Bandettini et al., 1994). Even at 3 T at least half the signal is extravascular in origin, and hence the gain in spatial specificity is minimal, whereas the loss in sensitivity is considerable (Jochimsen et al., 2004; Norris et al., 2002). Furthermore the relatively long TE required for optimal sensitivity in spin-echo fMRI leads to lengthy and hence sub-optimal TRs when combined with high spatial resolution in conventional spin-echo EPI sequences. The use of slice multiplexing (Larkman et al., 2001; Moeller et al., 2010) can potentially reduce the TR, but suffers from prohibitively high RF power deposition at high static magnetic field strengths. This could perhaps be alleviated by using parallel excitation arrays aligned to slices but these are still rather exotic. Variable rate (VERSE) RF pulses (Conolly et al., 1988) can also reduce power deposition but in the context of multiplexed pulses will likely be not as effective: the sum of multiple, phase-shifted pulses results in a very rapidly modulated RF envelope. In VERSE the amplitude modulations of the RF are minimised by modulating the slice selection gradient instead. Gradient slew-rates may prohibit the fast modulations of the original multiplexed RF envelope to be captured thereby reducing VERSE's potential for multiplexing. Furthermore, VERSE slice profiles degrade in the presence of off-resonance effects that increase with static magnetic field strength. In this study the power deposition problem was solved using the PINS technique (Norris et al., 2011). As demonstrated here this allows both high spatial resolution and a volume TR similar to that employed in conventional gradient-echo sequences. It will hence be possible to use spin-echo EPI at 7 T, and possibly at even higher main magnetic field strengths, for whole brain studies of both resting state connectivity, as demonstrated in the current article, and also for conventional activation studies.

As outlined above the main attraction of this method will be the high spatial specificity, whereby the lower signal contrast in comparison to a gradient echo sequence may well be ameliorated by the reduction in physiological noise that is implicit in the use of a spin-echo technique. To date there have been few publications utilising multiplexed imaging to examine BOLD signal changes (Feinberg et al., 2010; Smith et al., 2012), and it remains as yet unexplored to what extent leakage of signal between slices leads to artefactual measurement. The quality of the reconstruction is certainly very good, as evidenced by the high data quality presented in Fig. 1, however in the pursuit of subtle signal changes a small degree of leakage between slices may be sufficient to elevate a signal component above the threshold for statistical significance. The topics of sensitivity, specificity and leakage can only be addressed in dedicated studies that go beyond the scope of this article, however some insight is obtained from the current study.

First with regard to sensitivity, the results presented in this paper were obtained using just six subjects with slightly more than 15 min of scanning per subject. It is hence clear that the sensitivity is sufficient to perform studies with similar numbers of subjects and measurement durations to those conducted using gradient echo techniques. The good

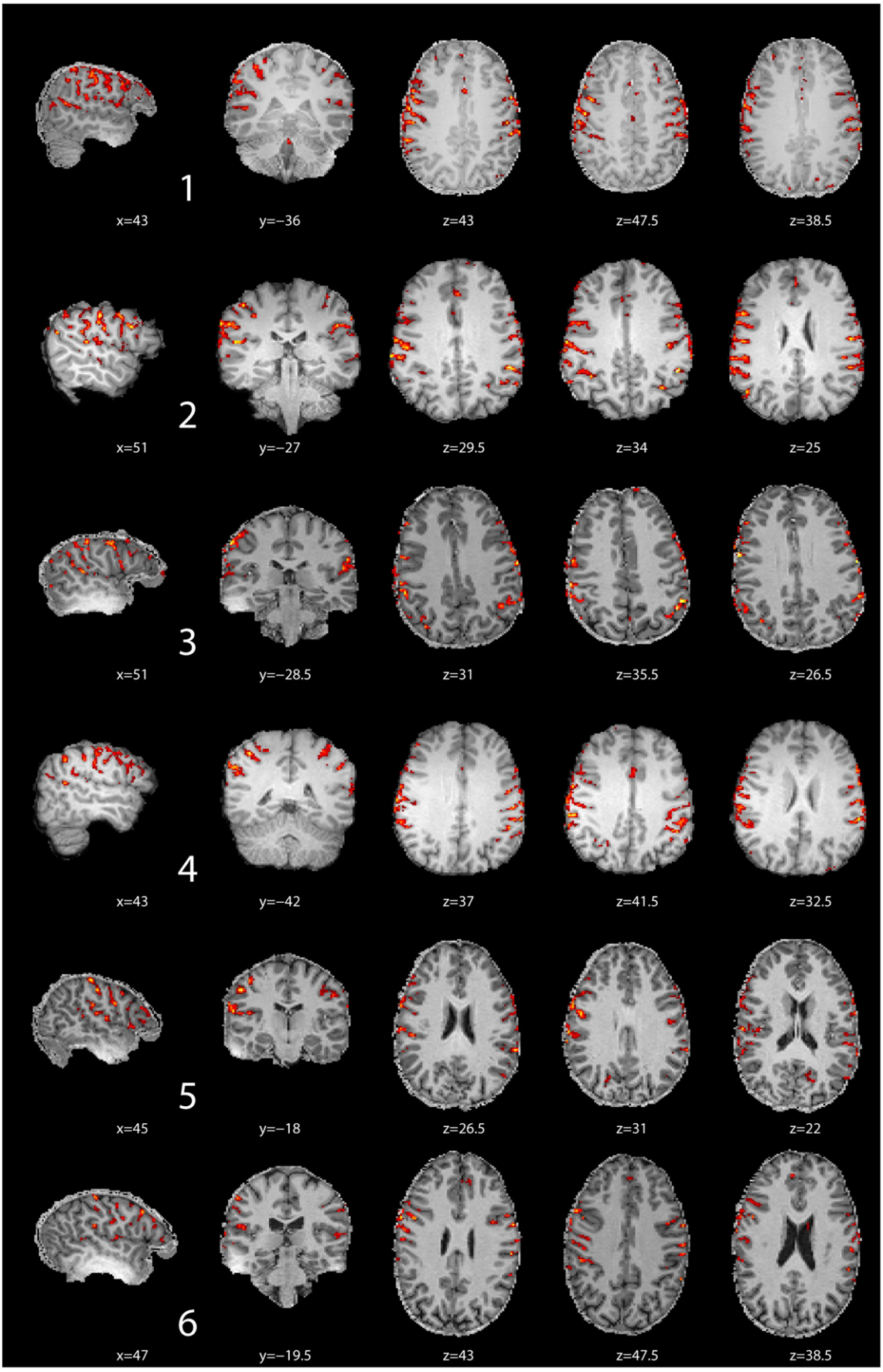

Fig. 6. Dual regression results of all subjects for somatosensory RSN (IC 28). High resolution, single subject activation patterns all show exquisite co-localisation with grey matter.

spatial specificity as documented by the results of the dual regression analysis may be of most value at the individual level, as group level analysis will inevitably require some smoothing to compensate for residual intersubject variability after normalisation to the group template and to comply with data normality and continuity requirements for parametric statistical tests. The dual regression method however allows one to return to the high resolution single subject space after group results have been established (Beckmann et al., 2009).

The benefit of the lack of signal voids is evident by examination of ICs 8, 22, 27 and 40 (shown in Fig. 2) which all show inferior medial frontal components in regions that are frequently not visible in gradient echo studies at a high magnetic field strengths. In the case of IC 8 we considered whether the lateral signal components could have arisen from signal leakage. We finally decided to retain the component on the basis that it was well localised to grey matter and similar to the ICs numbered 8 and 18 in the paper of Kiviniemi et al. (2009).

There are relatively few studies in the literature that have used such a large number of ICs in an ICA, and hence so far no consensus has been formed as to which components should be found. There are certainly differences between the present study and the ICs found in that of Kiviniemi et al. (2009), but there are differing numbers of volunteers, experimental durations, field strengths and contrasts, all of which may contribute to these. It is also well known from studies that use lower numbers of ICs that occasionally RSNs decompose into several component parts. From this perspective the differences between the two studies detract from the credibility of neither. Several of the RSNs found by Kiviniemi et al. can be approximated by summing ICs from the current study, for example Kiviniemi et al.'s IC6 is similar to the sum of ICs 24 and 31 in the current study. Furthermore in situations where there are known divisions of function, realistic RSNs are found in the present study: one example of which is the division of the visual system into medial (IC 53), occipital (IC 64) and lateral (IC 62) networks (shown in Fig. 1), another being the division of the language network into RSNs about BA44 (IC 13), BA45 (IC 25) and Wernicke's area (IC 29) that clearly exhibit the known left-lateralisation of language.

In conclusion, we have demonstrated that the combination of slice multiplexing and the PINS technique opens up new perspectives for spin-echo fMRI at 7 T, which should in future lead to increased use of this technique.

Acknowledgments

We would like to express our gratitude to Eelke Visser for providing the implementation of the geometric distortion correction algorithm. RB acknowledges financial support from the Dutch Ministerie van Economische Zaken, Provincie Overijssel and Provincie Gelderland via the ViP-BrainNetworks project.

References

Bandettini, P.A., Wong, E.C., Jesmanowicz, A., Hinks, R.S., Hyde, J.S., 1994. Spin-echo and gradient-echo EPI of human brain activation using BOLD contrast: a comparative study at 1.5 T. NMR Biomed. 7, 12–20.

Barth, M., Meyer, H., Kannengiesser, S.A., Polimeni, J.R., Wald, L.L., Norris, D.G., 2010. T2-weighted 3D fMRI using S2-SSFP at 7 Tesla. Magn. Reson. Med. 63, 1015–1020.

Beckmann, C.F., DeLuca, M., Devlin, J.T., Smith, S.M., 2005. Investigations into resting-state connectivity using independent component analysis. Philos. Trans. R Soc. Lond. B Biol. Sci. 360, 1001–1013.

Beckmann, C.F., Mackay, C.E., Filippini, N., Smith, S.M., 2009. Group comparison of resting-state FMRI data using multi-subject ICA and dual regression. 15th Annual Meeting of Organization for Human Brain Mapping. Neuroimage 47 (Supplement 1), S39–S41.

Blaimer, M., Breuer, F.A., Seiberlich, N., Mueller, M.F., Heidemann, R.M., Jellus, V., Wiggins, G., Wald, L.L., Griswold, M.A., Jakob, P.M., 2006. Accelerated volumetric MRI with a SENSE/GRAPPA combination. J. Magn. Reson. Imaging 24, 444–450.

Boxerman, J.L., Hamberg, L.M., Rosen, B.R., Weisskoff, R.M., 1995. MR contrast due to intravascular magnetic susceptibility perturbations. Magn. Reson. Med. 34, 555–566.

Chamberlain, R., Park, J.Y., Corum, C., Yacoub, E., Ugurbil, K., Jack Jr., C.R., Garwood, M., 2007. RASER: a new ultrafast magnetic resonance imaging method. Magn. Reson. Med. 58, 794–799.

Conolly, S., Nishimura, D., Macovski, A., Glover, G., 1988. Variable-rate selective excitation. J. Magn. Reson. 78, 440–458.

Constable, R.T., Kennan, R.P., Puce, A., McCarthy, G., Gore, J.C., 1994. Functional NMR imaging using fast spin echo at 1.5 T. Magn. Reson. Med. 31, 686–690.

Eickhoff, S.B., Paus, T., Caspers, S., Grosbras, M.H., Evans, A.C., Zilles, K., Amunts, K., 2007. Assignment of functional activations to probabilistic cytoarchitectonic areas revisited. Neuroimage 36, 511–521.

Feinberg, D.A., Moeller, S., Smith, S.M., Auerbach, E., Ramanna, S., Gunther, M., Glasser, M.F., Miller, K.L., Ugurbil, K., Yacoub, E., 2010. Multiplexed echo planar imaging for sub-second whole brain FMRI and fast diffusion imaging. PLoS One 5, e15710.

Goerke, U., van de Moortele, P.F., Ugurbil, K., 2007. Enhanced relative BOLD signal changes in T(2)-weighted stimulated echoes. Magn. Reson. Med. 58, 754–762.

Griswold, M.A., Jakob, P.M., Heidemann, R.M., Nittka, M., Jellus, V., Wang, J., Kiefer, B., Haase, A., 2002. Generalized autocalibrating partially parallel acquisitions (GRAPPA). Magn. Reson. Med. 47, 1202–1210.

Jenkinson, M., Bannister, P., Brady, M., Smith, S., 2002. Improved optimization for the robust and accurate linear registration and motion correction of brain images. Neuroimage 17, 825–841.

Jochimsen, T.H., Norris, D.G., Mildner, T., Moller, H.E., 2004. Quantifying the intra- and extravascular contributions to spin-echo fMRI at 3 T. Magn. Reson. Med. 52, 724–732.

Kiviniemi, V., Starck, T., Remes, J., Long, X., Nikkinen, J., Haapea, M., Veijola, J., Moilanen, I., Isohanni, M., Zang, Y.F., Tervonen, O., 2009. Functional segmentation of the brain cortex using high model order group PICA. Hum. Brain Mapp. 30, 3865–3886.

Larkman, D.J., Hajnal, J.V., Herlihy, A.H., Coutts, G.A., Young, I.R., Ehnholm, G., 2001. Use of multicoil arrays for separation of signal from multiple slices simultaneously excited. J. Magn. Reson. Imaging 13, 313–317.

Lee, S.P., Silva, A.C., Ugurbil, K., Kim, S.G., 1999. Diffusion-weighted spin-echo fMRI at 9.4 T: microvascular/tissue contribution to BOLD signal changes. Magn. Reson. Med. 42, 919–928.

Marques, J.P., Kober, T., Krueger, G., van der Zwaag, W., Van de Moortele, P.F., Gruetter, R., 2010. MP2RAGE, a self bias-field corrected sequence for improved segmentation and T1-mapping at high field. Neuroimage 49, 1271–1281.

Miller, K.L., Hargreaves, B.A., Lee, J., Ress, D., deCharms, R.C., Pauly, J.M., 2003. Functional brain imaging using a blood oxygenation sensitive steady state. Magn. Reson. Med. 50, 675–683.

Moeller, S., Yacoub, E., Olman, C.A., Auerbach, E., Strupp, J., Harel, N., Ugurbil, K., 2010. Multiband multislice GE-EPI at 7 Tesla, with 16-fold acceleration using partial parallel imaging with application to high spatial and temporal whole-brain fMRI. Magn. Reson. Med. 63, 1144–1153.

Norris, D.G., 2012. Spin-echo fMRI: the poor relation? Neuroimage 62 (2), 1109–1115.

Norris, D.G., Koopmans, P.J., Boyacioglu, R., Barth, M., 2011. Power independent of number of slices radiofrequency pulses for low-power simultaneous multislice excitation. Magn. Reson. Med. 66, 1234–1240.

Norris, D.G., Zysset, S., Mildner, T., Wiggins, C.J., 2002. An investigation of the value of spin-echo-based fMRI using a Stroop color-word matching task and EPI at 3 T. Neuroimage 15, 719–726.

Ogawa, S., Menon, R.S., Tank, D.W., Kim, S.G., Merkle, H., Ellermann, J.M., Ugurbil, K., 1993. Functional brain mapping by blood oxygenation level-dependent contrast magnetic resonance imaging. A comparison of signal characteristics with a biophysical model. Biophys. J. 64, 803–812.

Parkes, L.M., Schwarzbach, J.V., Bouts, A.A., Deckers, R.H., Pullens, P., Kerskens, C.M., Norris, D.G., 2005. Quantifying the spatial resolution of the gradient echo and spin echo BOLD response at 3 Tesla. Magn. Reson. Med. 54, 1465–1472.

Poser, B.A., Norris, D.G., 2007. Fast spin echo sequences for BOLD functional MRI. MAGMA 20, 11–17.

Scheffler, K., Seifritz, E., Bilecen, D., Venkatesan, R., Hennig, J., Deimling, M., Haacke, E.M., 2001. Detection of BOLD changes by means of a frequency-sensitive true FISP technique: preliminary results. NMR Biomed. 14, 490–496.

Smith, S.M., Fox, P.T., Miller, K.L., Glahn, D.C., Fox, P.M., Mackay, C.E., Filippini, N., Watkins, K.E., Toro, R., Laird, A.R., Beckmann, C.F., 2009. Correspondence of the brain's functional architecture during activation and rest. Proc. Natl. Acad. Sci. U. S. A. 106, 13040–13045.

Smith, S.M., Miller, K.L., Moeller, S., Xu, J., Auerbach, E.J., Woolrich, M.W., Beckmann, C.F., Jenkinson, M., Andersson, J., Glasser, M.F., Van Essen, D.C., Feinberg, D.A., Yacoub, E.S., Ugurbil, K., 2012. Temporally-independent functional modes of spontaneous brain activity. Proc. Natl. Acad. Sci. U. S. A. 109 (8), 3131–3136.

Studholme, C., Constable, R.T., Duncan, J.S., 2000. Accurate alignment of functional EPI data to anatomical MRI using a physics-based distortion model. IEEE Trans. Med. Imaging 19, 1115–1127.

Tomasi, D., Volkow, N.D., in press. Resting functional connectivity of language networks: characterization and reproducibility. Mol. Psychiatry. http://dx.doi.org/10.1038/mp.2011.177.

Uludag, K., Muller-Bierl, B., Ugurbil, K., 2009. An integrative model for neuronal activity-induced signal changes for gradient and spin echo functional imaging. Neuroimage 48, 150–165.

Varoquaux, G., Sadaghiani, S., Pinel, P., Kleinschmidt, A., Poline, J.B., Thirion, B., 2010. A group model for stable multi-subject ICA on fMRI datasets. Neuroimage 51, 288–299.

Visser, E., Qin, S., Zwiers, M.P., 2010. EPI distortion correction by constrained nonlinear coregistration improves group fMRI. Proceedings of the ISMRM, p. 3459.

Yacoub, E., Duong, T.Q., Van De Moortele, P.F., Lindquist, M., Adriany, G., Kim, S.G., Ugurbil, K., Hu, X., 2003. Spin-echo fMRI in humans using high spatial resolutions and high magnetic fields. Magn. Reson. Med. 49, 655–664.

Yarkoni, T., Poldrack, R.A., Nichols, T.E., Van Essen, D.C., Wager, T.D., 2011. Large-scale automated synthesis of human functional neuroimaging data. Nat. Methods 8, 665–670.